Monte Carlo Simulation for Radiative Transfer in a High-Pressure Industrial Gas Turbine Combustion Chamber

Tao Ren
Mem. ASME
School of Engineering,
University of California,
Merced, CA 95343
e-mail: tren@ucmerced.edu

Michael F. Modest[1]
Professor
Life Fellow ASME
School of Engineering,
University of California,
Merced, CA 95343
e-mail: mmodest@ucmerced.edu

Somesh Roy
Mem. ASME
Mechanical Engineering Department,
Marquette University,
Milwaukee, WI 53233
e-mail: somesh.roy@marquette.edu

Radiative heat transfer is studied numerically for reacting swirling flow in an industrial gas turbine burner operating at a pressure of 15 bar. The reacting field characteristics are computed by Reynolds-averaged Navier–Stokes (RANS) equations using the k-ϵ model with the partially stirred reactor (PaSR) combustion model. The GRI-Mech 2.11 mechanism, which includes nitrogen chemistry, is used to demonstrate the ability of reducing NO_x emissions of the combustion system. A photon Monte Carlo (PMC) method coupled with a line-by-line (LBL) spectral model is employed to accurately account for the radiation effects. Optically thin (OT) and PMC–gray models are also employed to show the differences between the simplest radiative calculation models and the most accurate radiative calculation model, i.e., PMC–LBL, for the gas turbine burner. It was found that radiation does not significantly alter the temperature level as well as CO_2 and H_2O concentrations. However, it has significant impacts on the NO_x levels at downstream locations. [DOI: 10.1115/1.4038153]

1 Introduction

In most gas turbine combustors, thermal radiation plays a major role to the heat transfer from the hot combustion products to the combustor walls, especially in luminous combustion where significant amount of soot particles are produced [1,2]. In modern stationary gas turbine combustor, air and fuel are premixed in a lean burning regime in order to achieve a homogenous temperature distribution, reduce NO_x and soot formation [3–7], and these gas turbines often operate at elevated pressures. Radiation may be important at higher pressure even in nonsooting flames as optical thickness of radiatively participating media is much larger.

Gas turbine combustion is a very complex process governed by a complicated turbulent flow field and strong effects of turbulence–chemistry interactions [2]. However, the rapid increase in computational power in recent years makes it possible to conduct reacting flow simulations using sophisticated turbulence models and detailed chemistry mechanisms [8–17]. However, adding detailed treatment of radiative heat transfer within such reacting flow simulations remains computationally very expensive. In these simulations, radiative heat transfer is either neglected [11–13,15] or simulated with very simple radiation models [9,10,14,16,17], which often leads to over- or underestimations of temperature fields. Radiation and chemistry are tightly coupled through the temperature, and correct temperature prediction considering radiation effects is required for correct prediction of all combustion species, in particular, NO_x. In modern gas turbine burners, swirl flames are used extensively to enable better mixing and high energy conversion [4,5,18]. In such burners, it was reported that with less than 0.1% of the energy released fluctuation is sufficient to generate pressure fluctuations having peak amplitudes equal to the mean chamber pressure [3]. Accurate prediction of radiative energy in the system is also critical to ensure combustion stability. Therefore, a high-fidelity radiation model is necessary to improve numerical predictions of the overall heat transfer in such systems.

The governing equation for radiative heat transfer in nongray participating media is given by the radiative transfer equation (RTE), which includes emission, absorption, and scattering. The RTE is an integro-differential equation for radiative intensity in six independent variables (three spatial, two directional, and one spectral). Consequently, the high dimensionality of RTEs prevents them from being solved exactly in general conditions [19]. The optically thin (OT) approximation for radiative heat transfer calculation was applied to several industrial gas turbine simulations recently [17,20]. This approximation ignores self-absorption and only gives total local emission from the medium and, therefore, overestimates the radiative heat loss. By transforming the RTE into a set of simultaneous partial differential equations, approximate solution methods were developed, such as the discrete ordinates method (DOM) and the spherical harmonics method (or PN method) [19]. The DOM is very popular in combustion solvers because of its ease of implementation and extension to high orders, and is commonly used for industrial combustor simulations with radiative heat transfer. Jones and Paul [9] combined DOM with large eddy simulation in a gas turbine combustor. The values for absorption coefficients (m^{-1}) of the radiatively participating medium were simply approximated as one tenth of mole fraction of CO_2 plus H_2O. Karalus [21] simulated a jet stirred reactor using DOM to account for radiation heat transfer from CO_2 and H_2O. No detail for the spectral information was given in the work and gases were assumed to be gray. Nemitallah and Habib [14] studied an atmospheric diffusion oxy-combustion flame in a gas turbine combustor applying DOM as the RTE solver with gray-gas assumption, applying the Planck-mean absorption coefficient. Kadar [22] investigated turbulent nonpremixed combustion in industrial furnaces using DOM with gray gas media. All these DOM calculations were implemented with very simple spectral models, mainly because of large computational cost of the method [19,23]. On the other hand, the lowest order spherical harmonics method, the P1 method, is relatively easy to implement and has reasonable computational efficiency. However, the P1 method is usually only accurate in media with near-isotropic radiative intensity, and is extremely difficult to be

[1]Corresponding author.

Contributed by the Combustion and Fuels Committee of ASME for publication in the Journal of Engineering for Gas Turbines and Power. Manuscript received May 16, 2017; final manuscript received August 16, 2017; published online December 12, 2017. Assoc. Editor: Song-Charng Kong.

extended to high orders due to the complicated mathematics involved. Only a few numerical simulations for industrial combustor have applied the P1 method as the RTE solver to account for radiative heat transfer [22,24–26].

The photon Monte Carlo (PMC) method solves the RTE in a stochastic manner, which directly mimics the physical processes by releasing representative energy bundles (rays) into random directions, which are traced until they are absorbed at certain points in the medium or escape from the domain. This allows the accurate treatment of the complications in radiative heat transfer modeling, such as nongray spectral properties, inhomogeneous media, and irregular geometries, with relative ease. The PMC method, while computationally expensive, can readily be implemented with the line-by-line (LBL) spectral model without significantly increasing computational cost compared to gray calculations [27,28]. The LBL spectral model resolves all individual spectral lines and is the most accurate spectral model, which can be combined with PMC (PMC–LBL) to serve as benchmark for other RTE solvers and spectral models. When increasing the number of energy bundles, the PMC–LBL results will approach the exact LBL solution with diminishing statistical error.

In the present work, the PMC–LBL radiation model was applied to study the radiative heat transfer for reacting swirling flow in an industrial gas turbine combustor operating at a pressure of 15 bar [29]. The simulated gas turbine combustor is the Siemens SGT-100, which premixes air and natural gas in a swirler prior to burning to introduce better mixing and resulting in a lean burning regime with low NO_x emissions [30]. The original-sized industrial gas turbine burner and combustion chamber of SGT-100 were installed in a high-pressure test rig at German Aerospace Center (DLR) in Stuttgart, Germany and operated with natural gas and preheated air at pressures up to 6 bar [31]. Experimental investigations have been conducted on the combustor for quantification of flow field, composition, and temperature [6,31,32]. Reynolds-averaged Navier–Stokes (RANS) and large eddy simulations have been performed to the experimental version of the gas turbine combustor with different turbulent combustion models and chemistry mechanisms [15,17,18,20,33,34]. However, no detailed treatment for radiative heat transfer was included in any of these simulations.

It should be noted that the purpose of this study is not to resolve flame details quantitatively with sophisticated turbulence and combustion models, but to demonstrate the radiation effects in industrial gas turbine combustion with a high-fidelity radiation model. The authors were not able to obtain all the details of the geometry and operating conditions for the SGT-100 combustor because of technical confidentiality issues [6]. Therefore, there were no intentions to simulate the experimental gas turbine combustion chamber operating at relatively lower pressures to resolve all the flame details quantitatively. Without detailed information, such as geometry and operating conditions, quantitative prediction of temperature and other quantities, which can match with experimental measurements, would be impossible and that is also beyond the scope of our studies. The dimensions of the combustor were obtained from Stopper and Meier's experimental work [31]. The flow conditions were scaled to the turbine operating pressure of 15 bar from case D (6 bar) in their experimental measurements. The reacting swirling flow was simulated on a simplified two-dimensional (2D) axisymmetric geometry by RANS simulations with the standard k-ϵ turbulence model. The partially stirred reactor (PaSR), which has been extensively used for gas-turbine like combustor simulations, was also applied here for turbulent combustion modeling. The reaction chemistry was described using the detailed GRI-Mech 2.11 chemical mechanism [35], which is designed to model natural gas combustion, consisting of 227 elementary reactions among 49 species and including NO formation. A newly generated high-pressure LBL database, specifically applied to PMC calculation [36], was used for the radiative heat transfer modeling. CO_2, H_2O, and CO were assumed to be the only radiatively participating species and wall radiation was considered as well. Results from optically thin and gray-gas calculations coupled with flow and combustion simulation were also presented for comparison.

2 Mathematical Models

2.1 Governing Equations. In the RANS context, conservation equations (continuity, momentum, species, and enthalpy) can be written in terms of Favre averages [37]. The Favre-averaged continuity equation is given by

$$\frac{\partial \overline{\rho}}{\partial t} + \frac{\partial (\overline{\rho}\tilde{u}_j)}{\partial x_j} = 0 \tag{1}$$

where the over bar $(-)$ denotes the Reynolds averaging while the tilde $(\sim)$ denotes the Favre-averages. The Favre-averaged momentum equation is given by

$$\frac{\partial (\overline{\rho}\tilde{u}_i)}{\partial t} + \frac{\partial (\overline{\rho}\tilde{u}_i\tilde{u}_j)}{\partial x_j} = -\frac{\partial \overline{p}}{\partial x_i} + \frac{\partial}{\partial x_j}\left(\overline{\tau}_{ij} - \overline{\rho u_i'' u_j''}\right) \tag{2}$$

where τ_{ij} is the viscous stress. In the averaging procedure, the Reynolds stress terms of $-\overline{\rho u_i'' u_j''}$ are introduced, which are unclosed and have to be modeled by a turbulence model. The Favre-averaged species transport equation for species s is given by

$$\frac{\partial (\overline{\rho}\tilde{Y}_s)}{\partial t} + \frac{\partial (\overline{\rho}\tilde{Y}_s\tilde{u}_j)}{\partial x_j} = \frac{\partial}{\partial x_j}\left(\overline{\rho} D_s \frac{\partial \tilde{Y}_s}{\partial x_j} - \overline{\rho Y_s'' u_j''}\right) + \tilde{\dot{\omega}}_s \quad s = 1, \ldots\ldots, m \tag{3}$$

where D_s is the mass diffusivity, $\tilde{\dot{\omega}}_s$ is the Favre-averaged chemical reaction rate, and m is the total number of species in the system. The Favre-averaged energy equation is given by

$$\frac{\partial (\overline{\rho}\tilde{h})}{\partial t} + \frac{\partial \left(\overline{\rho}\tilde{h}\tilde{u}_j\right)}{\partial x_j} = \frac{\partial}{\partial x_j}\left(\overline{\rho}\alpha \frac{\partial \tilde{h}}{\partial x_j} - \overline{\rho h'' u_j''}\right) + \overline{S_h} + \overline{S_{\text{rad}}} \tag{4}$$

where α is the thermal diffusivity. The two averaged terms $\overline{S_h}$ and $\overline{S_{\text{rad}}}$ are the chemical and radiative heat sources, respectively. In this study, turbulence–chemistry interaction is considered to close the chemical reaction rate term and chemical heat source term by combustion models. However, turbulence–radiation interaction is neglected, i.e., $\overline{S_{\text{rad}}} = S_{\text{rad}}$ and is calculated by radiation models.

2.2 Turbulence Model. In addition to the Reynolds stress term $-\overline{\rho u_i'' u_j''}$ in Eq. (2), the other two unclosed terms $-\overline{\rho Y_s'' u_j''}$ and $-\overline{\rho h'' u_j''}$, in Eqs. (3) and (4), referred to as Reynolds flux terms, have to also be modeled. In the present study, closure for these terms in the government equations was achieved using the standard k-ϵ model [38]. By introducing the turbulent viscosity μ_t, the Reynolds stress term is expressed as [39]

$$-\overline{\rho u_i'' u_j''} = \mu_t\left(\frac{\partial \tilde{u}_i}{\partial x_j} - \frac{\partial \tilde{u}_j}{\partial x_i} - \frac{2}{3}\delta_{ij}\frac{\partial \tilde{u}_k}{\partial x_k}\right) + \frac{2}{3}\overline{\rho} k \delta_{ij} \tag{5}$$

where δ_{ij} is the Kronecker delta and k is the Favre-averaged turbulent kinetic energy. The turbulent viscosity can be calculated as

$$\mu_t = C_u \overline{\rho}\frac{k^2}{\tilde{\epsilon}} \tag{6}$$

where C_u is a model constant and $\tilde{\epsilon}$ is the Favre-averaged dissipation rate of turbulence kinetic energy. Two additional transport equations for the Favre-averaged turbulent kinetic energy and

dissipation rate are solved in order to close the Reynolds stress term. A more detailed discussion concerning these two equations may be found in Refs. [22] and [40]. The Reynolds flux terms in Eqs. (3) and (4) are closed by applying gradient diffusion assumptions, i.e.,

$$-\overline{\rho Y_s'' u_j''} = \frac{\mu_t}{\mathrm{Sc}_s^t}\frac{\partial \tilde{Y}_s}{\partial x_j}, \quad -\overline{\rho h'' u_j''} = \frac{\mu_t}{\mathrm{Pr}_h^t}\frac{\partial \tilde{h}}{\partial x_j} \tag{7}$$

where Sc_s^t and Pr_h^t are turbulent Schmidt number for species s and turbulent Prandtl number for enthalpy, respectively.

2.3 Combustion Model. The reaction rate, as expressed by the Arrhenius law with temperature in the exponent, is a highly nonlinear term [41]. The Favre-averaged reacting rate $\tilde{\dot{\omega}}_s$ in Eq. (3) can never be directly evaluated as a function of averaged species mass fractions, densities, and temperature, which have to be modeled by the combustion model. In the present study, the partially stirred reactor combustion model is applied to model the turbulence–combustion interaction. In the PaSR approach, a computational cell is split into two different parts: a reacting part and a nonreacting part. The reacting part is treated as a perfectly stirred reactor, in which the composition is homogenously reacted and mixed. After reactions have taken place, the species are mixed due to turbulence for the mixing time τ_{mix}, and the resulting concentration gives the final concentration in the entire, partially stirred cell. The reader is referred to Refs. [22] and [42–44] for more details. By using the PaSR model, the Favre-averaged reaction rate is calculated as

$$\tilde{\dot{\omega}}_s = k_s \dot{\omega}_s \tag{8}$$

where $\dot{\omega}_s$ is the laminar reaction rate calculated using the detailed chemical kinetic mechanism GRI-Mech 2.11 for species s, and k_s is the reactive fraction of the reactor cell, which is calculated from

$$k_s = \frac{\tau_c}{\tau_c + \tau_{\mathrm{mix}}} \tag{9}$$

where τ_c is the chemical time-scale determined by solving the coupled ordinary differential equations governing the chemical kinetics. The turbulence mixing time-scale τ_{mix} is obtained from the k-ϵ model as [45]

$$\tau_{\mathrm{mix}} = C_{\mathrm{mix}}\sqrt{\frac{(\mu + \mu_t)}{\overline{\rho}\tilde{\epsilon}}} \tag{10}$$

where C_{mix} is a parameter that can be used to scale the turbulence mixing time-scale. In the present work, the default value of $C_{\mathrm{mix}} = 0.1$ was used. After the Favre-averaged reaction rate is obtained, the chemical heat source in Eq. (4) is evaluated as

$$\overline{S_h} = \sum_{s=1}^{m} \Delta\overline{h_s}\,\tilde{\dot{\omega}}_s \tag{11}$$

where $\overline{h_s}$ is the species formation enthalpy, which is obtained from the detailed chemical kinetic mechanism GRI-Mech 2.11.

2.4 Radiation Model. In order to calculate the local radiative heat source S_{rad} in Eq. (4), the RTE has to be solved with species spectral properties to obtain local radiative intensity [19]. For this gas turbine simulation, a finite volume-based PMC–LBL model was used. In the PMC analysis, photon bundles are emitted in random directions from random locations in each computational cell. The interaction between photon bundles and cells (i.e., absorption) is evaluated commensurate with the optical thickness that a photon bundle travels through a cell. Thus, the RTE is solved to provide the local radiative heat source of a cell by balancing the energy emitted and absorbed in a cell, and wall heat flux by radiation may be obtained by collecting all the photon bundles hitting and leaving wall boundaries.

In PMC calculations, the emitting location, direction, and wavenumber of a photon bundle must be determined in a statistically meaningful way. So-called random-number relations were developed to obtain statistically meaningful locations, directions, and wavenumbers of emitting photon bundles [19,27]. A random-number relation determining the emitting location of a photon bundle was developed according to the emissive energy distribution in the domain, i.e., a "hot" emitting zone is more likely to release more photon bundles than a "cold" absorbing zone. For an isotropic medium, photon bundles should be randomly released into all directions with equal probability; a random-number relation for emission direction was developed to ensure photon bundles are released "isotropically." For gray gas analysis with the PMC method, the Planck-mean absorption coefficient is used for calculations: all photon bundles carry identical absorption coefficients and no spectral model is required. However, the combustion products such as CO_2, H_2O, and CO are highly nongray, which only emit and absorb across a few spectral bands with strong spectral variations of radiative properties. Due to the rapid increase in computational power, conducting line-by-line calculations, the most accurate radiative heat transfer simulation has become possible. Wang and Modest [27] developed random-number relations for LBL accurate spectral Monte Carlo models. By using random-number relations, the wavenumbers with substantial emission are more likely to be chosen. Therefore, fewer photon bundles are required to yield accuracy comparable to the one obtained from standard spectral integration. Based on Wang's work, Ren and Modest [28] developed a new wavenumber selection scheme, which displays a significant improvement in computational efficiency, and thus is employed in the present study. In this scheme, when a random number for emitting wavenumber, R_η, is drawn, the emitting species is determined first; then the emitting wavenumber and the corresponding absorption coefficient are determined from a tabulated random-number wavenumber relation database, which has the form of

$$R_{\eta,s} = f(P,T,x_s,\eta), \kappa_{\eta,s} = f(P,T,x_s,\eta), \quad s = 1,\ldots\ldots,m \tag{12}$$

where P is total pressure, x_s are mole fraction of species s and $\kappa_{\eta,s}$ is the absorption coefficient. Ren and Modest [36] built a database tabulating these relations for CO_2, H_2O, CO, CH_4, C_2H_4, and soot for a temperature range from 300 K to 3000 K, and total pressures ranging from 0.1 bar to 80 bar from LBL spectroscopic databases [46,47] to cover most conditions found in industrial practice. In the present study, CO_2, H_2O, and CO (no significant amount of soot is generated due to the lean-premixed combustion in swirling flow) are assumed to be the only radiatively participating species and wall radiation is considered as well.

3 Computational Details

The SGT-100 is an industrial gas turbine with approximately 5 MW output with a pressure ratio of approximately 15:1 [28]. Although the detailed geometrical features of the SGT-100 combustor were not released, the original-sized experimental version of the gas turbine combustor gives some detail as in Fig. 1 [31]. The system consists of a main burner, pilot burner, radial swirler, and double-skinned can combustor. German natural gas (containing 96.97% of CH_4) is mixed with preheated air in the radial swirler and passes through the swirler vanes into the combustion chamber. All the gases are assumed to be an "ideal gas" and obey the "ideal gas law." In the simulation, CH_4 is considered as the combustion fuel and the swirler is not included in the simulation. The swirling flow is generated by enforcing a tangential velocity to the inlet flow according to the 60 deg swirler vane angle,

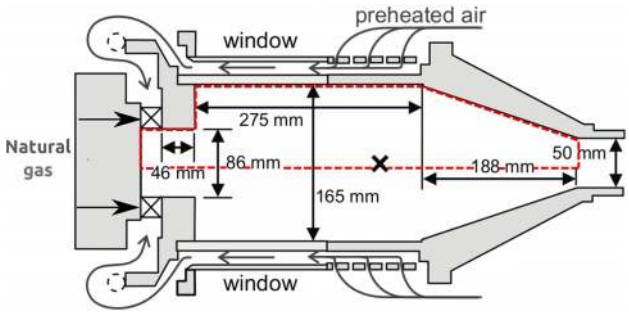

Fig. 1 The industrial burner with combustion chamber of the SGT-100 [31]

assuming air and CH_4 are well premixed passing the swirler. The 2D axisymmetric computational domain (confined within the red-dash lines) is indicted in Fig. 1, including flow inlet, combustor walls, and flow outlet. The computational grid and boundaries are shown in Fig. 2. The reacting compressible flow solver is built on OpenFOAM [48], an open-source computational fluid dynamics (CFD) software. OpenFOAM uses the finite volume method with unstructured mesh topology. A wedge is the most common way to represent an axisymmetric full cylinder in the finite volume CFD simulation. Thus, the 2D axisymmetric domain was specified as a 5 deg three-dimensional wedge, and one cell thick running along the plane of symmetry. Cyclic boundary conditions are applied to an axisymmetric wedge geometry with approximately 15,000 cells. Prior to the inlet, CH_4 and air are premixed in the swirler at flow rates of 0.049 kg/s and 1.3875 kg/s, respectively. The mixture has a temperature of 400 °C at the burner inlet. All walls are assumed to be black and diffuse with fixed temperatures of 400 °C, governed by the temperature of the cooling air. RANS equations were solved with the standard k-ϵ model, the PaSR combustion model with detailed reaction mechanism GRI-Mech 2.11, and radiation models.

4 Results and Discussions

4.1 Grid Independence. A grid independence study was conducted first to ensure numerically error-free results. The current mesh of approximately 15,000 cells was refined in both directions, resulting in a refined mesh size of approximately 40,000 cells. The reacting swirling flow was simulated on both meshes without any radiation model involved. The simulation results from the two different grid systems are found to be in good agreement with each other for flow fields, temperatures, and species compositions. The axial velocity, temperature, and CO mass fraction distributions at one axial ($x = 0.1$ m) and one radial ($r = 0.03$ m) locations of the combustion fields are compared for the two grid systems in Fig. 3: the refined mesh does not result in any considerable variations in the results. Thus, the current mesh is considered to be grid independent.

4.2 Flow Patterns and Overall Flame Characteristics. Computed steady-state mean velocity magnitude contour with superimposed pseudo-streamlines (on the $x - r$ plane based on the mean axial and radial velocity components), temperature, CO_2, H_2O, and CO mass fraction contours are shown in Fig. 4. These results were obtained with the PMC–LBL radiation model. The fresh fuel–air mixture passes through the swirler vane (inlet) and turns through a right angle into the combustion chamber, followed by sudden expansion. A smaller outer recirculation zone develops in the corner of the combustion chamber due to the confined geometry of the burner. Under effects of the swirling flow, the vortex breakdown leads to formation of a larger inner recirculation zone, which is critical for flame stabilization. Similar flow patterns were also observed in early observations of confined swirling flows [3,12,32]. The inner recirculation drives the hot combustion products back to the flame root and mixes them with the incoming fuel–air mixture. The swirling flow introduces better mixing of combustion products and efficient energy transport, resulting in a relatively uniform temperature distribution inside the combustion chamber. The combustion products like CO_2 and H_2O are distributed pretty much uniformly at downstream locations with high concentrations. The maximum CO mass fraction is about 1%, and has significantly lower levels downstream. The mean CO mass fraction contour indicates the flame position in the combustor. It can be seen that combustion takes place between the two recirculation zones, where turbulence is intense and the flame is short and thin. Within the larger IRZ, where the residence time is long, turbulence is weak, the temperature remains relatively high. The higher level of turbulence near the flame zone and lower levels of turbulence downstreams were observed by previous experimental measurements and large eddy simulations calculations [15,17,18].

4.3 Radiation Effects on Combustion. Radiation models coupled with a reacting flow solver are likely to yield different combustion environments and to affect temperature and species composition distribution as opposed to scenarios without considering radiation. The flame shapes calculated without any radiation feedback (NoRad) and with OT, PMC–gray, and PMC–LBL radiation models are illustrated by the temperature profiles given in Fig. 5. Without considering radiation, there is zero radiative heat loss from the hot combustion products. At the other extreme, when using the OT approximation, self-absorption of the radiatively participating medium is ignored and maximum radiation heat loss is obtained. With PMC–gray or PMC–LBL, the emitted photon bundles will be (partially or totally) absorbed by the medium along the path. Normally, NoRad predicts the overall highest temperatures and OT predicts the lowest temperature level; temperatures calculated by any other radiation models are expected to be between these two extremes. As shown in Fig. 5, due to the maximum radiative heat loss, with the OT radiation model, the smallest hot temperate zone ($T > 1900$ K) is predicted. For the PMC–gray model, due to some reabsorption, it predicts a slightly smaller hot temperature zone compared to the results obtained without radiation. For this gas turbine combustor, the PMC–LBL predicts the largest hot temperature zone and temperatures are higher than without considering radiation over most parts of the downstream locations. The temperature profiles predicted by different models along the radial direction near the burner exit

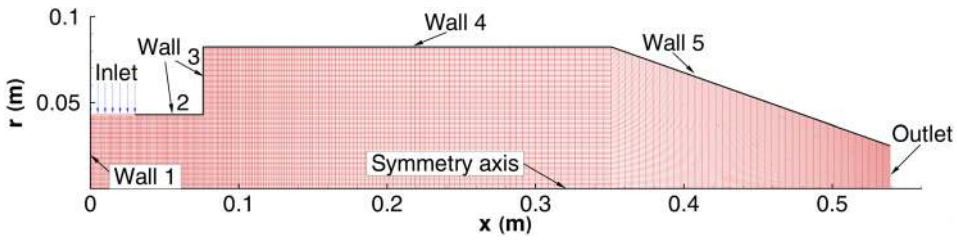

Fig. 2 Computational mesh and boundaries for the gas turbine combustor

($x = 0.5$ m) are shown in Fig. 6. With the OT radiation model, the maximum temperature drops about 80 K. However, using the PMC–LBL radiation model, maximum temperature actually rises about 10 K. The PMC–gray model predicts a lower temperature compared to NoRad calculation. NO_x formation is very sensitive to the maximum temperature in combustion, and the slightly higher temperature predicted with PMC–LBL model results in a higher NO_x mass fraction, which is also shown in Fig. 6.

In order to understand why the PMC–LBL radiation model predicts higher temperature than without considering radiation, the mean mass fraction contours of the combustion radical OH from NoRad and PMC–LBL calculations are shown in Fig. 7, to demonstrate the radiation effects on combustion. Although the temperature differences are not huge when comparing NoRad and PMC–LBL calculations, the flame shapes are quite different. For this gas turbine combustor, the two major radiatively participating species, CO_2 and H_2O, are distributed pretty much uniformly at downstream locations with high concentrations. Results by PMC–LBL show that about 80% of the total emission from the medium has been reabsorbed. Because of the long distance effects from radiation, we speculate that the flame may be affected by radiation from its high temperature and high concentration of radiatively participating species at downstream locations. Combustion may be enhanced by the reabsorption process and result in a different flame shape and higher temperature. This is indeed the case and also is indicated in Fig. 7, where a larger value of maximum OH mass fractions is predicted by PMC–LBL calculations. This is also demonstrated by the volume-averaged CO_2, H_2O, and CO

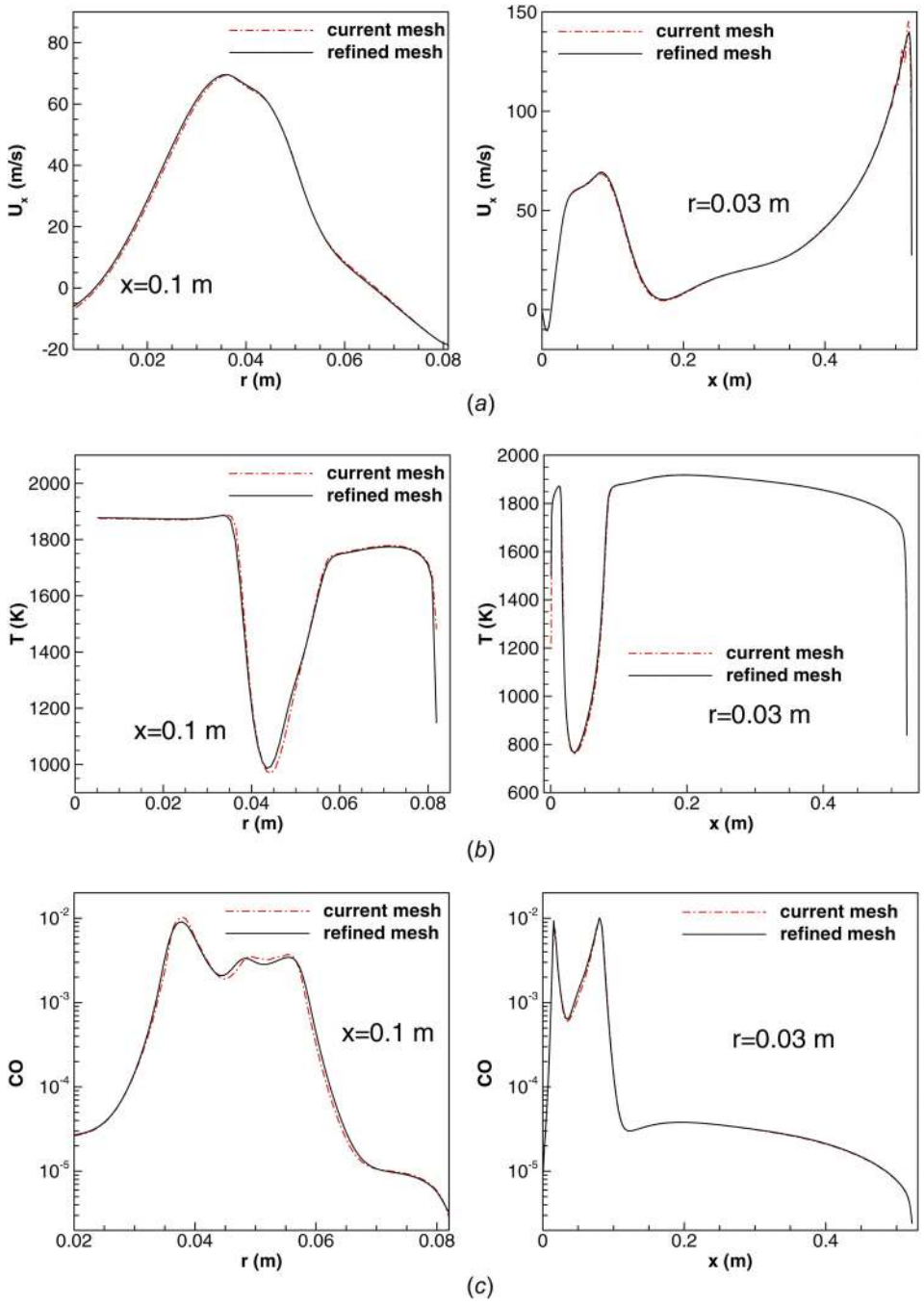

Fig. 3 The comparison of the axial velocity, temperature, and CO mass fraction distributions calculated with current mesh of approximately 15,000 cells and refined mesh of approximately 40,000 cells

mass fractions, as shown in Fig. 8. With PMC–LBL, more CO_2, H_2O, and less CO are produced; combustion is enhanced and is more complete with the effect of strong reabsorption of radiation. Although the temperature calculated by PMC–LBL model is higher than NoRad calculation, the enthalpy within the system should be always between the enthalpies calculated with OT and NoRad. The volume-integrated enthalpy in the computational domain is also shown in Fig. 8, indicating that the enthalpy calculated with PMC–LBL model is indeed between the two extremes of OT and NoRad.

The net radiative heat fluxes on the combustor walls have also been calculated with different radiation models, which are shown in Fig. 9 (refer to Fig. 2 for wall indices). Although the size of the combustor chamber is not very large, CO_2 and H_2O are distributed relatively uniformly downstream with higher mass fractions at a higher pressure, which makes the optical thickness of the radiatively participating medium much larger. According to the PMC–LBL predictions, the heat fluxes to the walls due to radiation were not significant, i.e., only about 20% of the radiative emission reaches the combustor walls. On the other hand, that

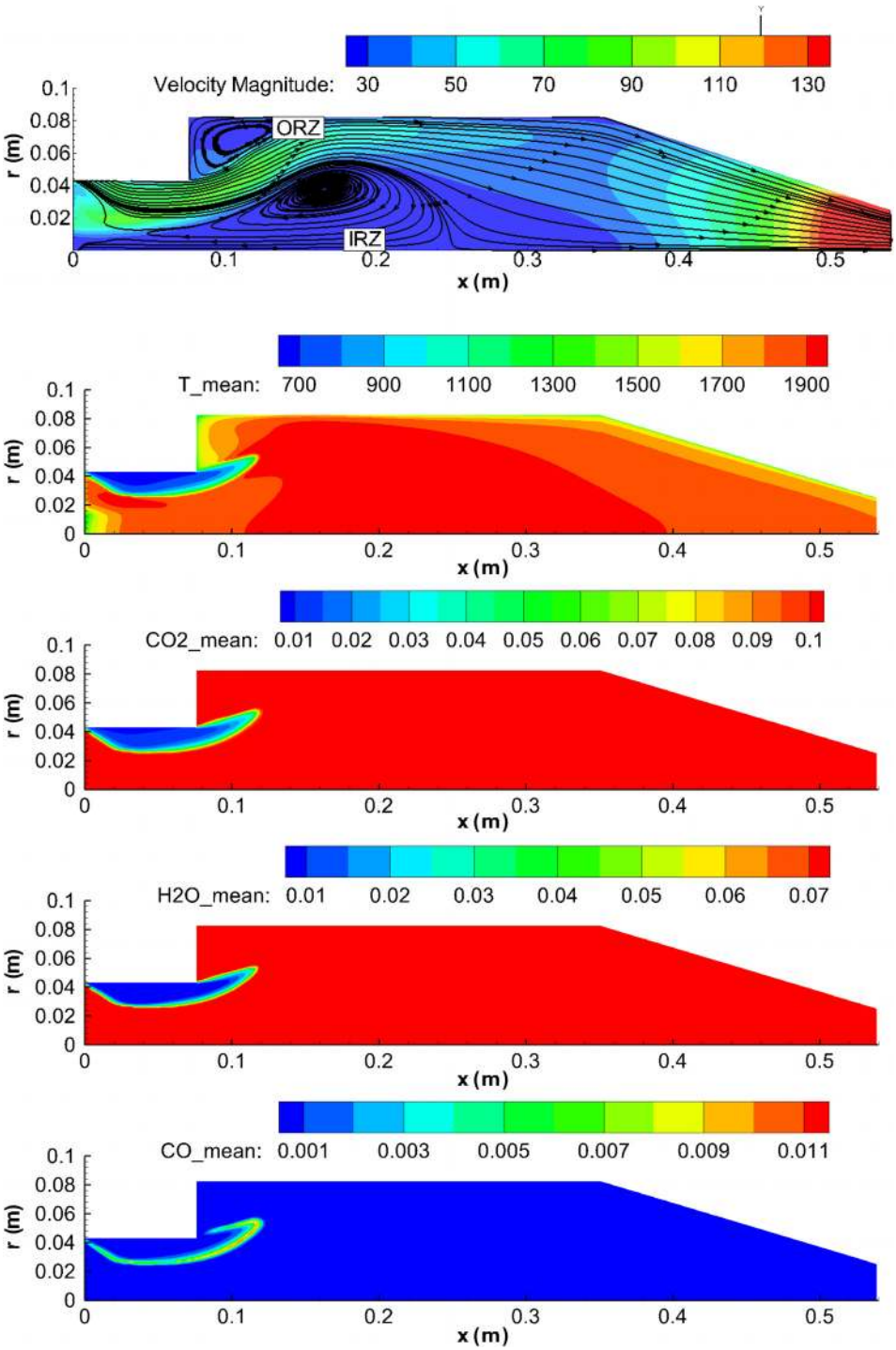

Fig. 4 Steady-state mean velocity magnitude (m/s) superimposed with pseudo-streamlines, temperature (in kelvin), CO_2, H_2O, and CO mass fraction contours calculated with PMC–LBL radiation model for the gas turbine combustion burner

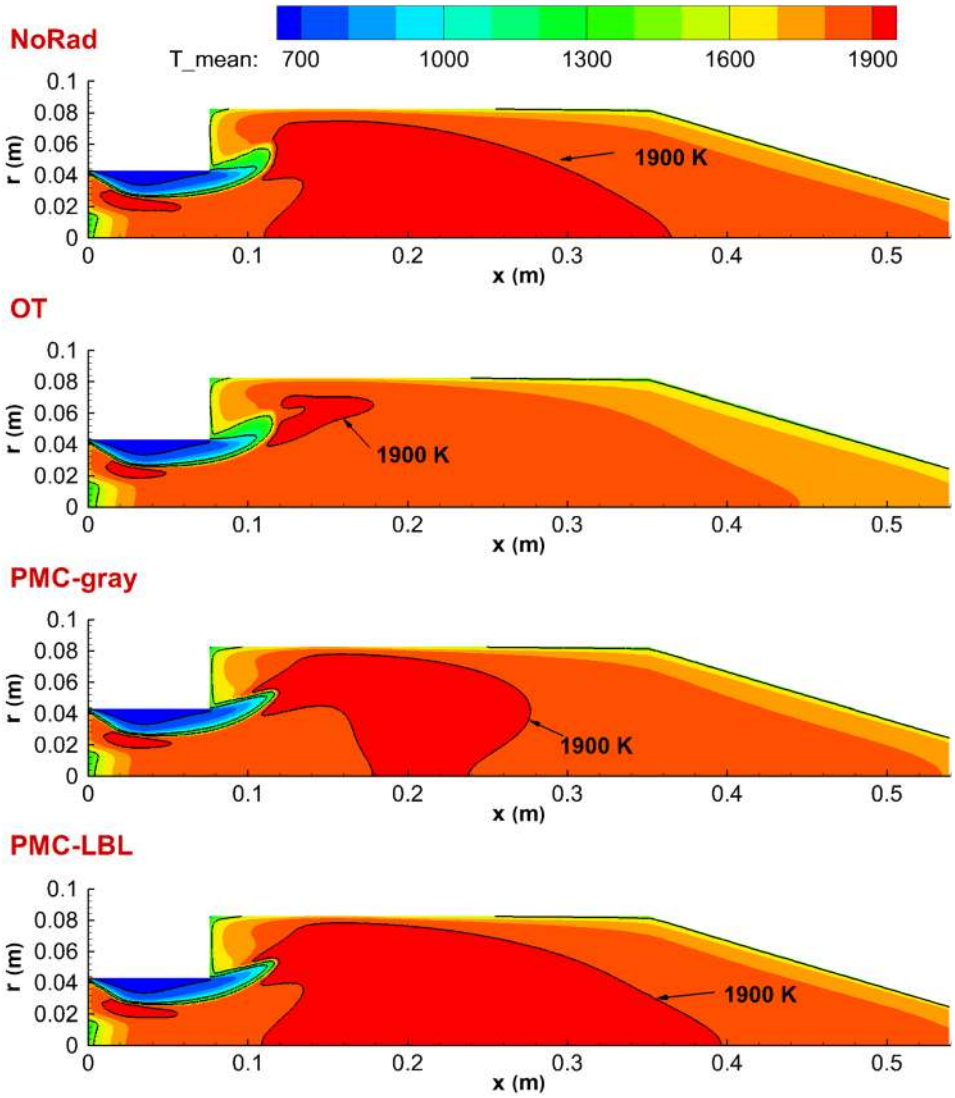

Fig. 5 Temperature (in kelvin) profiles calculated without radiation (NoRad) feedback, with OT, PMC-gray, and PMC–LBL radiation models for the gas turbine combustion

means the radiative heat fluxes to the walls are vastly overestimated by the OT method, since all self-absorption is neglected. For radiatively participating gases, such as CO_2, H_2O, and CO, the absorption coefficients oscillate wildly within few spectral bands across the electromagnetic spectrum. Therefore, the gray-gas assumption may often lead to very significant errors in the analysis. The radiative heat fluxes are also overestimated by PMC–gray calculation, as shown in Fig. 9.

4.4 Computational Cost for PMC–LBL Radiation Model. The PMC–LBL radiation model solves the nongray RTE and provides the radiative heat source S_{rad} to the energy equation of Eq.

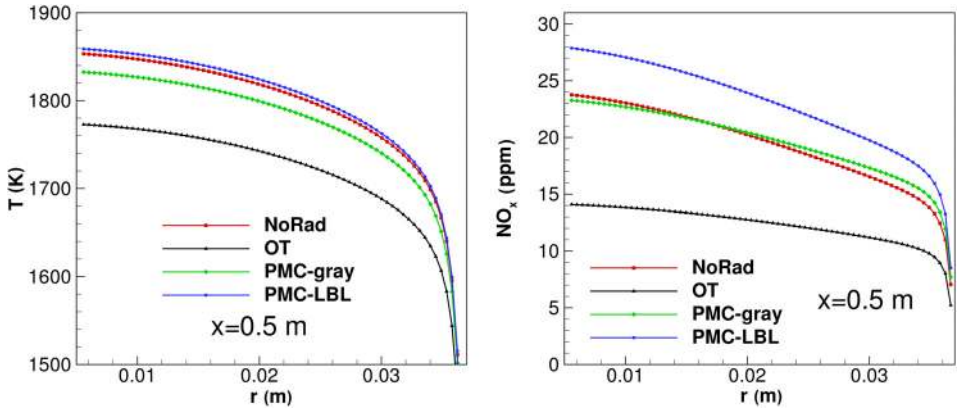

Fig. 6 Temperature (in kelvin) and NO_x mass fraction near the gas turbine burner exit

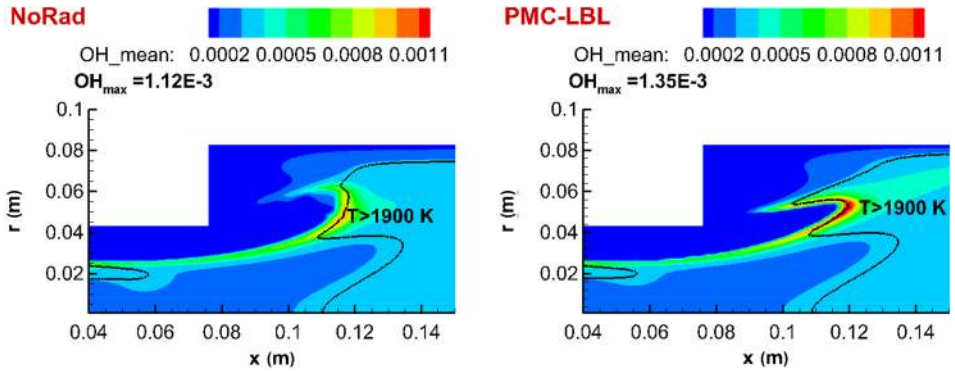

Fig. 7 The mean mass fraction contours of OH calculated without radiation (NoRad) feedback and with PMC–LBL radiation for the gas turbine combustion burner

(4). Since the PMC is statistical in nature, it yields a slightly different solution from time-step to time-step. To minimize this variation, a large number of photon bundles can be released and traced, but this would be computationally very expensive. In the multiscale simulation of combustion, the time-step is often determined by chemical models; the change of the mean-flow field is much more slowly compared to the small time steps needed for accurate chemical reaction modeling. Without considering turbulence radiation interaction, the radiative heat source term is only controlled by the mean-flow field and also changes much more slowly, it is not necessary to solve the RTE at every time-step. Instead of running a large number of photon bundles at every time-step, tempered averaging may be used, with relatively few photon bundles at every time-step, combined with time-blending over steps, i.e., an updated radiative heat source is evaluated from Refs. [23], [49], and [50]

$$S^{*}_{\text{rad}} = \alpha S^{n-1}_{\text{rad}} + (1-\alpha) S^{n}_{\text{rad}} \tag{13}$$

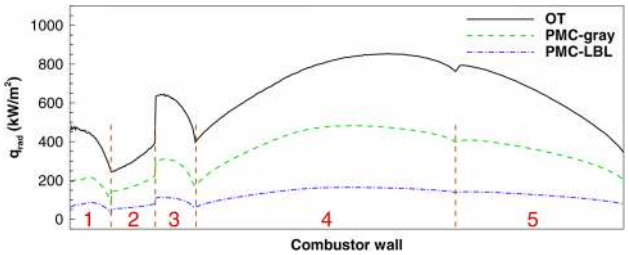

Fig. 9 The net radiative heat fluxes on the combustor walls

where α is a time-blending factor with a relatively large value, the superscript n–1 denotes previous time-step, n represents current time-step, and S^{*}_{rad} is the radiative heat source calculated at time-step n using relatively few photon bundles with time-blending. In the present study for PMC–LBL calculations, 100,000 photon

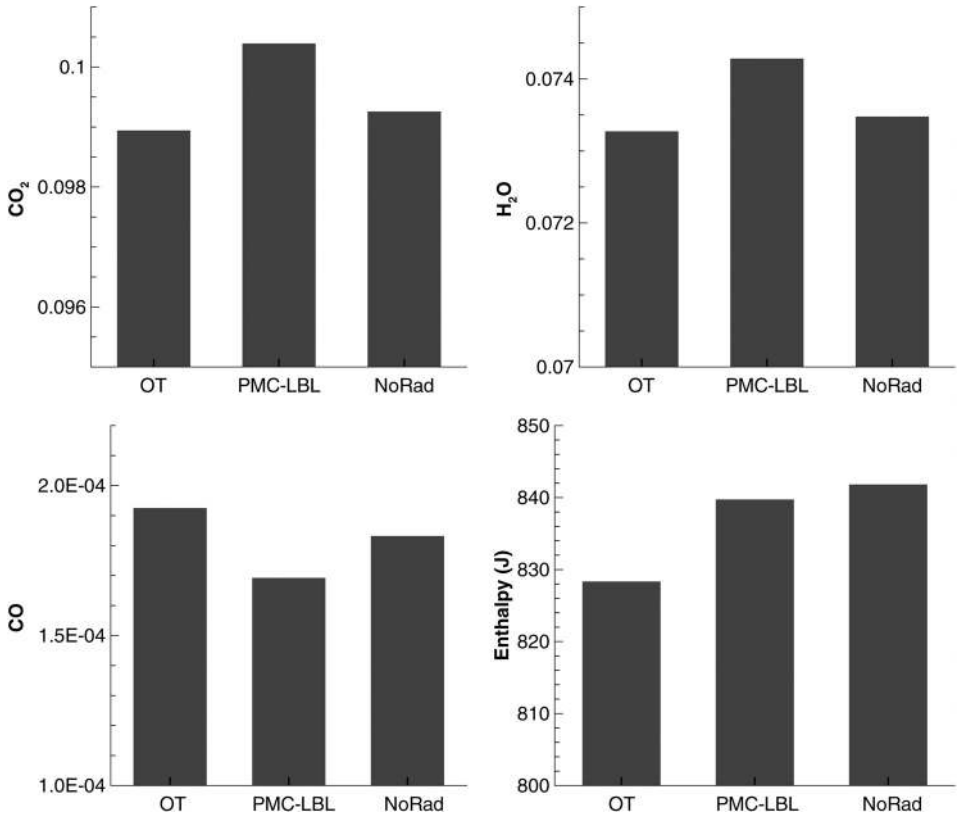

Fig. 8 Volume-averaged CO_2, H_2O, and CO mass fractions and volume-integrated enthalpy and in the computational domain

bundles are released at each time-step. A time-blending factor $\alpha = 0.999$ is used in Eq. (13) to include the impact of more histories in the average. By using this setup, comparing against no radiation calculation, the PMC–LBL radiation model costs about 16.5% more central processing unit time, and the standard error for the total radiative heat loss is estimated to be about 1% of the mean value.

5 Conclusions

In the present study, existing turbulence and combustion models were coupled with an improved, more realistic, high-fidelity radiation model, PMC–LBL, to simulate an industrial gas turbine burner operating at a pressure of 15 bar with reacting swirling flow. Results obtained by applying OT and PMC–gray radiation models were also presented for comparison. The local mean flow, temperature, and combustion species fields are computed by solving RANS equations with the k-ϵ turbulence model and the PaSR combustion model. The detailed natural gas–air reaction mechanism of GRI-Mech 2.11 was applied to describe combustion kinetics.

The combustion simulations conducted with the most accurate high-fidelity radiation model PMC–LBL indicate that combustion may be enhanced by the reabsorption of the emission from the radiatively participating combustion products, which predicted a different flame shape and higher temperate than without considering radiation effects. PMC–LBL calculations resulted higher downstream temperatures and NO_x level. Results obtained with different radiation models also indicated that for this gas turbine combustion, due to the relatively large optical thickness of combustion products at higher pressure, optically thin and gray calculations vastly overestimate the radiative heat losses, resulting in overestimated radiative heat flux to the combustor walls. When the radiative participating media have uniform and strong concentrations in a high-pressure gas turbine combustor, this results in strong reabsorption through the media, and it is important to use the PMC–LBL radiation model, in order to accurately predict temperature distribution and NO_x emission.

Funding Data

- Air Force Office of Scientific Research (AFOSR Contract No. FA8650-15-C-2543).
- National Science Foundation (NSF/DOE Collaborative Research Award No. 1258635).

Nomenclature

C_u = k-ϵ model constant
C_{mix} = PaSR model constant
D_s = mass diffusivity for species s, m^2/s
h = enthalpy, J/kg
k = turbulent kinetic energy, m^2/s^2
P = pressure, bar
Pr = Prandtl number
q = heat flux, W/m^2
R_η = random number for emitting wavenumber
Sc = Schmidt number
S_h = chemical heat source, W/m^3
S_{rad} = radiative heat source, W/m^3
t = time, s
T = temperature, K
u_j = velocity, m/s
x_j = spatial coordinate, m
x_s = mole fraction of species s
Y_s = mass fraction of species s

Greek Symbols

α = thermal diffusivity, m^2/s
δ_{ij} = Kronecker delta
ϵ = turbulent dissipation rate, m^2/s^3
η = wavenumber, cm^{-1}
κ_η = absorption coefficient, cm^{-1}
μ_t = turbulent viscosity, kg/m · s
ρ = density, kg/m^3
τ_c = chemical time-scale, s
τ_{mix} = turbulence mixing time-scale, s
τ_{ij} = viscous stress, Pa
$\dot{\omega}$ = gas species production rates, $kg/m^3 \cdot s$

Acronyms

LBL = line-by-line
NoRad = no radiation
OT = optically thin
PaSR = partially stirred reactor
PMC = photon Monte Carlo
RANS = Reynolds-averaged Navier–Stokes
RTE = radiative transfer equation

References

[1] Lefebvre, A. H., 1984, "Flame Radiation in Gas Turbine Combustion Chambers," Int. J. Heat Mass Transfer, **27**(9), pp. 1493–1510.
[2] Lefebvre, A. H., and Ballal, D. R., 2010, *Gas Turbine Combustion: Alternative Fuels and Emissions*, CRC Press, Boca Raton, FL.
[3] Huang, Y., 2003, "Modeling and Simulation of Combustion Dynamics in Lean-Premixed Swirl-Stabilized Gas-Turbine Engines," Ph.D. thesis, The Pennsylvania State University, State College, PA.
[4] Weigand, P., Meier, W., Duan, X. R., Stricker, W., and Aigner, M., 2006, "Investigations of Swirl Flames in a Gas Turbine Model Combustor—I: Flow Field, Structures, Temperature, and Species Distributions," Combust. Flame, **144**(1), pp. 205–224.
[5] Meier, W., Duan, X. R., and Weigand, P., 2006, "Investigations of Swirl Flames in a Gas Turbine Model Combustor—II: Turbulence–Chemistry Interactions," Combust. Flame, **144**(1), pp. 225–236.
[6] Stopper, U., Aigner, M., Ax, H., Meier, W., Sadanandan, R., Stöhr, M., and Bonaldo, A., 2010, "PIV, 2D-LIF and 1D-Raman Measurements of Flow Field, Composition and Temperature in Premixed Gas Turbine Flames," Exp. Therm. Fluid Sci., **34**(3), pp. 396–403.
[7] Benini, E., 2013, *Progress in Gas Turbine Performance*, InTech, Rijeka, Croatia.
[8] Mallampalli, H. P., Fletcher, T. H., and Chen, J. Y., 1998, "Evaluation of CH_4/NO_x Reduced Mechanisms Used for Modeling Lean Premixed Turbulent Combustion of Natural Gas," ASME J. Eng. Gas Turbines Power, **120**(4), pp. 703–712.
[9] Jones, W. P., and Paul, M. C., 2005, "Combination of DOM with LES in a Gas Turbine Combustor," Int. J. Eng. Sci., **43**(5), pp. 379–397.
[10] Amaya, J., Collado, E., Cuenot, B., and Poinsot, T., 2010, "Coupling LES, Radiation and Structure in Gas Turbine Simulations," Summer Program of the Center for Turbulence Research, Stanford, CA, June 26–July 23.
[11] Joung, D., and Huh, K. Y., 2010, "3D RANS Simulation of Turbulent Flow and Combustion in a 5 MW Reverse-Flow Type Gas Turbine Combustor," ASME J. Eng. Gas Turbines Power, **132**(11), p. 111504.
[12] Gicquel, L. Y., Staffelbach, G., and Poinsot, T., 2012, "Large Eddy Simulations of Gaseous Flames in Gas Turbine Combustion Chambers," Prog. Energy Combust. Sci., **38**(6), pp. 782–817.
[13] Abou-Taouk, A., Sadasivuni, S., Lörstad, D., and Eriksson, L., 2013, "Evaluation of Global Mechanisms for LES Analysis of SGT-100 DLE Combustion System," ASME Paper No. GT2013-95454.
[14] Nemitallah, M. A., and Habib, M. A., 2013, "Experimental and Numerical Investigations of an Atmospheric Diffusion Oxy-Combustion Flame in a Gas Turbine Model Combustor," Appl. Energy, **111**, pp. 401–415.
[15] Bulat, G., Jones, W. P., and Marquis, A. J., 2013, "Large Eddy Simulation of an Industrial Gas-Turbine Combustion Chamber Using the Sub-Grid PDF Method," Proc. Combust. Inst., **34**(2), pp. 3155–3164.
[16] Donini, A. A., 2014, "Advanced Turbulent Combustion Modeling for Gas Turbine Application," Ph.D. thesis, Technische Universiteit Eindhoven, Eindhoven, The Netherlands.
[17] Bulat, G., Jones, W. P., and Marquis, A. J., 2014, "NO and CO Formation in an Industrial Gas-Turbine Combustion Chamber Using LES With the Eulerian Sub-Grid PDF Method," Combust. Flame, **161**(7), pp. 1804–1825.
[18] Bulat, G., Jones, W. P., and Navarro-Martinez, S., 2015, "Large Eddy Simulations of Isothermal Confined Swirling Flow in an Industrial Gas-Turbine," Int. J. Heat Fluid Flow, **51**, pp. 50–64.
[19] Modest, M. F., 2013, *Radiative Heat Transfer*, 3rd ed., Academic Press, New York.
[20] Bulat, G., Fedina, E., Fureby, C., Meier, W., and Stopper, U., 2015, "Reacting Flow in an Industrial Gas Turbine Combustor: LES and Experimental Analysis," Proc. Combust. Inst., **35**(3), pp. 3175–3183.
[21] Karalus, M. F., 2013, "An Investigation of Lean Blowout of Gaseous Fuel Alternatives to Natural Gas," Ph.D. thesis, University of Washington, Seattle, WA.
[22] Kadar, A. H., 2015, "Modelling Turbulent Non-Premixed Combustion in Industrial Furnaces," Ph.D. thesis, Delft University of Technology, Delft, The Netherlands.

[23] Cai, J., Lei, S., Dasgupta, A., Modest, M. F., and Haworth, D. C., 2014, "High Fidelity Radiative Heat Transfer Models for High-Pressure Laminar Hydrogen–Air Diffusion Flames," Combust. Theory Modell., **18**(6), pp. 607–626.
[24] Sun, L., Zheng, Q., Li, Y., Luo, M., and Bhargava, R. K., 2012, "Numerical Simulation of a Complete Gas Turbine Engine With Wet Compression," ASME J. Eng. Gas Turbines Power, **135**(1), p. 012002.
[25] Prieler, R., Demuth, M., Spoljaric, D., and Hochenauer, C., 2014, "Evaluation of a Steady Flamelet Approach for Use in Oxy-Fuel Combustion," Fuel, **118**, pp. 55–68.
[26] Rajhi, M. A., Ben-Mansour, R., Habib, M. A., Nemitallah, M. A., and Andersson, K., 2014, "Evaluation of Gas Radiation Models in CFD Modeling of Oxy-Combustion," Energy Convers. Manage., **81**, pp. 83–97.
[27] Wang, A., and Modest, M. F., 2007, "Spectral Monte Carlo Models for Nongray Radiation Analyses in Inhomogeneous Participating Media," Int. J. Heat Mass Transfer, **50**(19–20), pp. 3877–3889.
[28] Ren, T., and Modest, M. F., 2013, "Hybrid Wavenumber Selection Scheme for Line-by-Line Photon Monte Carlo Simulations in High-Temperature Gases," ASME J. Heat Transfer, **135**(8), p. 084501
[29] Siemens AG, 2005, "SGT-100 Industrial Gas Turbine," Siemens AG, Munich, Germany, accessed Oct. 13, 2017, https://www.siemens.com/global/en/home/products/energy/power-generation/gas-turbines/sgt-100.html#!/
[30] Igoe, B. M., 2011, "Dry Low Emissions Experience Across the Range of Siemens Small Industrial Gas Turbines," Siemens Industrial Turbomachinery Limited, Lincoln, UK.
[31] Stopper, U., Meier, W., Sadanandan, R., Stöhr, M., Aigner, M., and Bulat, G., 2013, "Experimental Study of Industrial Gas Turbine Flames Including Quantification of Pressure Influence on Flow Field, Fuel/Air Premixing and Flame Shape," Combust. Flame, **160**(10), pp. 2103–2118.
[32] Stopper, U., Aigner, M., Meier, W., Sadanandan, R., Stöhr, M., and Kim, I. S., 2009, "Flow Field and Combustion Characterization of Premixed Gas Turbine Flames by Planar Laser Techniques," ASME J. Eng. Gas Turbines Power, **131**(2), p. 021504
[33] Abou-Taouk, A., Sadasivuni, S., Lörstad, D., Ghenadie, B., and Eriksson, L., 2015, "CFD Analysis and Application of Dynamic Mode Decomposition for Resonant-Mode Identification and Damping in an SGT-100 DLE Combustion System," Seventh European Combustion Meeting, Budapest, Hungary, Mar. 30–Apr. 2, Paper No. P4–46.
[34] Abou-Taouk, A., Farcy, B., Domingo, P., Vervisch, L., Sadasivuni, S., and Eriksson, L.-E., 2016, "Optimized Reduced Chemistry and Molecular Transport for Large Eddy Simulation of Partially Premixed Combustion in a Gas Turbine," Combust. Sci. Technol., **188**(1), pp. 21–39.
[35] Bowman, C. T., Hanson, R. K., Davidson, D. F., Gardiner, W. C., Lissianski, V., Smith, G. P., Golden, D. M., Frenklach, M., and Goldenberg, M., 1995, "GRI-Mech 2.11," University of California, Berkeley, CA, accessed Oct. 13, 2017, http://www.me.berkeley.edu/gri_mech
[36] Ren, T., and Modest, M. F., 2017, "Line-by-Line Random-Number Database for Monte Carlo Simulations of Radiation in Combustion System," ICHMT International Symposium on Advances in Computational Heat Transfer (CHT), Napoli, Italy, May 28–June 1, Paper No. CHT-17-69.
[37] Poinsot, T., and Veynante, D., 2005, *Theoretical and Numerical Combustion*, 2nd ed., R. T. Edwards, Philadelphia, PA.
[38] Launder, B. E., and Spalding, D. B., 1974, "The Numerical Computation of Turbulent Flows," Comput. Methods Appl. Mech. Eng., **3**(2), pp. 269–289.
[39] Schmitt, F. G., 2007, "About Boussinesq's Turbulent Viscosity Hypothesis: Historical Remarks and a Direct Evaluation of Its Validity," C. R. Méc., **335**(9), pp. 617–627.
[40] Versteeg, H. K., and Malalasekera, W., 2007, *An Introduction to Computational Fluid Dynamics: The Finite Volume Method*, Pearson Education, London.
[41] Echekki, T. M. E., 2010, *Turbulent Combustion Modeling: Advances, New Trends and Perspectives*, Vol. 95, Springer Science & Business Media, Berlin.
[42] Tanahashi, M., Fujimura, M., and Miyauchi, T., 2000, "Coherent Fine-Scale Eddies in Turbulent Premixed Flames," Proc. Combust. Inst., **28**(1), pp. 529–535.
[43] Sabel'Nikov, V. A., and da Silva, L. F. F., 2002, "Partially Stirred Reactor: Study of the Sensitivity of the Monte Carlo Simulation to the Number of Stochastic Particles With the Use of a Semi-Analytic, Steady-State, Solution to the PDF Equation," Combust. Flame, **129**(1), pp. 164–178.
[44] Sabelnikov, V., and Fureby, C., 2013, "LES Combustion Modeling for High Re Flames Using a Multi-Phase Analogy," Combust. Flame, **160**(1), pp. 83–96.
[45] Kärrholm, P. F., 2008, "Numerical Modeling of Diesel Spray Injection, Turbulence Interaction and Combustion," Ph.D. thesis, Chalmers University of Technology, Gothenburg, Sweden.
[46] Rothman, L. S., Gordon, I. E., Barber, R. J., Dothe, H., Gamache, R. R., Goldman, A., Perevalov, V. I., Tashkun, S. A., and Tennyson, J., 2010, "HITEMP, the High-Temperature Molecular Spectroscopic Database," J. Quant. Spectrosc. Radiat. Transfer, **111**(15), pp. 2139–2150.
[47] Rothman, L. S., Gordon, I. E., Babikov, Y., Barbe, A., Benner, D. C., Bernath, P. F., Birk, M., Bizzocchi, L., Boudon, V., Brown, L. R., Campargue, A., Chance, K., Cohen, E. A., Coudert, L. H., Devi, V. M., Drouin, B. J., Fayt, A., Flaud, J. M., Gamache, R. R., Harrison, J. J., Hartmann, J. M., Hill, C., Hodges, J. T., Jacquemart, D., Jolly, A., Lamouroux, J., Le Roy, R. J., Li, G., Long, D. A., Lyulin, O. M., Mackie, C. J., Massie, S. T., Mikhailenko, S., Müller, H. S. P., Naumenko, O. V., Nikitin, A. V., Orphal, J., Perevalov, V., Perrin, A., Polovtseva, E. R., Richard, C., Smith, M. A. H., Starikova, E., Sung, K., Tashkun, S., Tennyson, J., Toon, G. C., Tyuterev, VI. G., and Wagner, G., 2013, "The HITRAN2012 Molecular Spectroscopic Database," J. Quant. Spectrosc. Radiat. Transfer, **130**, pp. 4–50.
[48] OpenCFD, 2013, "Version2.2.x, OpenFOAM Website," OpenCFD Ltd., Bracknell, UK, accessed Oct. 13, 2017, https://github.com/OpenFOAM/OpenFOAM-2.2.x
[49] Bissel, D., 1994, *Statistical Methods for SPC and TQM*, Chapman and Hall, New York.
[50] Feldick, A. M., and Modest, M. F., 2012, "A Spectrally Accurate Tightly-Coupled 2-D Axisymmetric Photon Monte Carlo RTE Solver for Hypersonic Entry Flows," ASME J. Heat Transfer, **134**(12), p. 122701.